

A robot system for medical ultrasound

S.E. Salcudean, W.H. Zhu, P. Abolmaesumi, S. Bachmann and P.D. Lawrence
Department of Electrical and Computer Engineering
University of British Columbia
Vancouver, BC, V6T 1Z4, Canada
{tims@ee.ubc.ca}

Abstract

A teleoperation approach to diagnostic ultrasound, in which the ultrasound transducer is positioned by a robot, is described in this paper. An inherently safe counterbalanced robot has been designed and tested in carotid artery examinations. The feasibility of using visual servoing for motion in the plane of the ultrasound probe has also been demonstrated using a modified image correlation algorithm and feature tracking algorithms. Research issues that have arisen in developing this and other systems designed for human augmentation are also presented.

1 Introduction

Robotics has an increasingly important role to play in the development of human augmentation systems. Such systems can address tasks that can only be accomplished with marginal success by people, or at the cost of work related injuries. Medical assistive devices and robots have been proposed for endoscopic surgery, microsurgery, rehabilitation, etc., and promise to significantly change healthcare delivery in a number of important areas.

Motivated initially by the need to avoid the repeated musculoskeletal injuries that ultrasound technicians are suffering [16, 4], the authors have embarked upon the development of a teleoperation system for medical ultrasound. The system consists of a joystick/haptic interface, a slave manipulator carrying the ultrasound probe, and a computer control system that allows the operator to remotely position the ultrasound transducer on the patient's body. The problem considered first as a test-bed for robot-assisted ultrasound is that of carotid artery examination, carried out to detect occlusive disease in the left and right common carotid arteries - a major cause of strokes.

A robot-assisted ultrasound examination system

would provide other benefits, such as the ability to collect and optimize 3-D ultrasound images [1], the ability to provide guidance to interventions (e.g., percutaneous pericardial puncture) and register images. Teleradiology is another possibility - although a number of methods for transmitting ultrasound images have been proposed in the literature [13], none allow the radiologist to view *and manipulate* the ultrasound transducer at the remote site.

Research issues that need to be addressed in order to make such a system work are discussed in this paper. Robot system requirements are summarized in Section 2.1, with a suitable robot design and haptic interface being presented in Section 2.2. Unilateral and bilateral control are discussed in Section 3, including the feasibility of controlling the transducer using ultrasound image servoing. Research challenges are discussed in Section 4, where the particular issues that arise in designing human augmentation systems are discussed. Conclusions and plans for future work follow.

The proposed robot-assisted ultrasound examination system has been discussed before in [11]. In this paper, the control, design and image tracking aspects have been expanded, while other aspects have been omitted. A similar system has been proposed recently in [7].

2 Electromechanical design

2.1 Ultrasound robot performance

An ultrasound transducer was fitted with an electromagnetic position and orientation sensor (ATC The BirdTM) and a JR³ force/torque sensor. Errors in the measurement setup were quantified and found to be minimal for orientation measurements and acceptable in translation because of design safety margins.

During a carotid artery examination, the patient lies

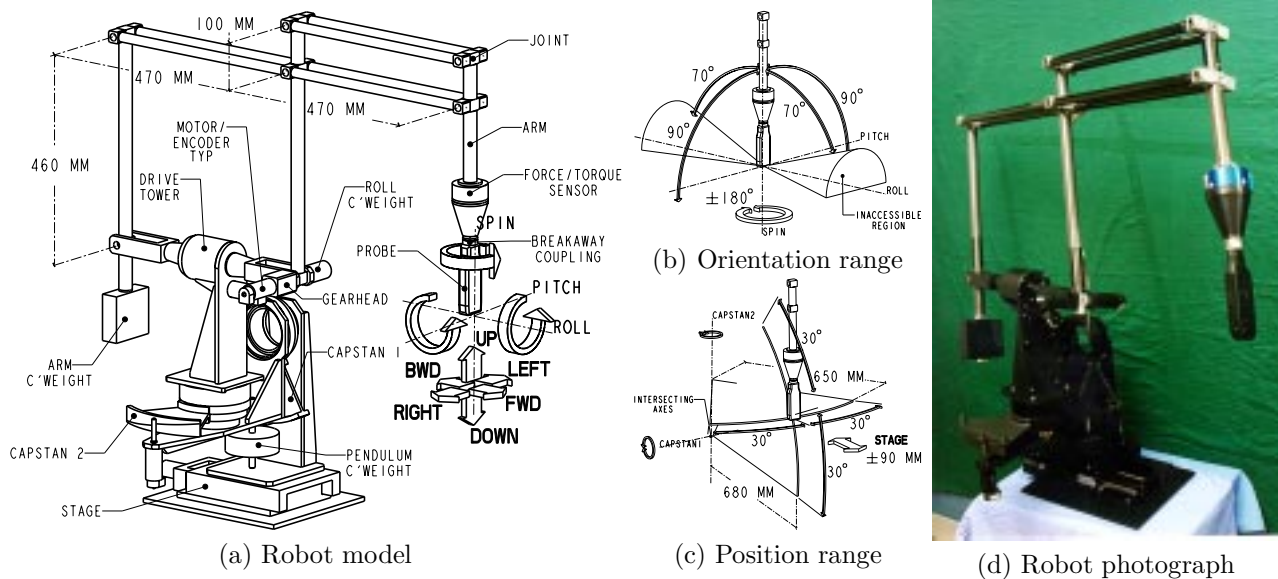


Figure 1: Ultrasound robot schematic, probe motion range, and robot photograph.

Axis	Transmission ratio	Resolution		Equivalent Mass*	Force/Torque	
		(Calculated)	(Experimental)		Force	Force**
X	40:1	0.026 mm	< 0.2 mm	2.13 kg	15.5 N	9.0 N
Y	2.02 $\frac{\text{mm}}{\text{rad}}$	0.003 mm	< 0.1 mm	20.1 kg	130 N	10.0 N
Z	40:1	0.027 mm	< 0.2 mm	1.64 kg	15.5 N	9.0 N
Rotation					Torque	Torque**
Pitch	50:1	0.2°	--	0.68 kg·m ²	13.1 Nm	2.5 Nm
Roll	93.6:1	0.2°	--	0.63 kg·m ²	24.6 Nm	2.5 Nm
Spin	1:1	0.1°	--	10 ⁻⁵ kg·m ²	0.15 Nm	0.15 Nm

Table 1: Ultrasound robot characteristics. * Along principal axes at nominal position. ** Software and hardware (D/A range, current gain, fuse) limited.

on a bed facing up, while the examiner scans the distal end of the common carotid artery and the proximal ends of the internal and external carotid arteries, both longitudinally and transversely, from the clavicle to the mandible on both the left and right sides of the neck.

The measurements are tabulated in [11]. The translation range is less than 15 cm in each direction, while the orientation range is quite well approximated by a right elliptical cone in which the probe must tilt $\pm 75^\circ$ about the patient's neck axis, and less than $\pm 50^\circ$ about the patient's shoulder axis. The probe must attain all these positions and orientations with an arbitrary rotation about its longitudinal axis.

The maximum velocities recorded, of the order of 0.2 m/s and $260^\circ/\text{s}$, occurred during a switch to a different scanning area or during probe re-orientation. The

average velocities were very small, of the order of 5 mm/s and $3^\circ/\text{s}$.

Probe forces are less than 6.5 N, while torques vary from 0.1 to 0.7 N·m, with 0.1 N·m occurring about the ultrasound probe longitudinal axis.

2.2 Ultrasound robot design

A robot used for ultrasound probe positioning must be safe under any circumstance, including power failure, and should move fast enough to allow the ultrasound examination to take place at a pace close to that achieved by the unassisted sonographer. Therefore, the robot should be light and of limited force ability. The robot joints should be backdriveable so that the arm could be pushed out of the way if necessary and controlled effectively in force mode. In addition, the robot should cover the required range of mo-

tions and forces required by the task. Because of the large orientation workspace required, the orientation and translation of the probe tip should be approximately decoupled, to avoid arm displacement solely to accommodate probe orientation changes.

A number of design options, such as the use of a spherical wrist, were eliminated by testing whether the range of required orientations could be attained without interference and with reasonable link lengths. The only remote-center wrist structure that was found to satisfy the orientation range requirement was a rotating parallelogram linkage as used in the LARS robot [14]. The parallelogram linkage used in this design is different because of the need to counterbalance the arm.

The robot design is presented in Fig. 1. The robot is placed at the head of the bed, with the labeled FWD and BWD directions being aligned with the bed longitudinal axis. Note that the parallelogram wrist is rolled to one side or the other during most of the carotid artery examination, and therefore most of the probe normal force is controlled by capstan 2, which moves the least mass and therefore allows for higher bandwidth force-control.

Three adjustable counterweights were used to fully balance the robot. The roll and arm counterweights place the center of mass of the parallelogram linkage at a fixed point on the linkage roll axis, independently of the ultrasound transducer orientation. Because of mechanical interference (e.g. between the arm counterweight and the capstan), the roll axis had to be placed above capstan 1, creating an unstable inverted pendulum with the center of mass above the capstan 1 axis. This center of mass of this pendulum was moved below the capstan 1 axis by a pendulum counterweight.

As seen in Fig. 1 (b),(c), the ultrasound transducer workspace significantly exceeds the specified requirements.

2.3 Haptic interface

A desk-top magnetically levitated haptic interface called PowerMouse has been developed that is suitable for controlling the ultrasound probe while providing force feedback to the operator [9]. Its electromechanical design is summarized in Figure 2. The device has a handle attached to a cubic “flotor” structure with the flat coils of six Lorentz actuators embedded in its faces. Twenty-four magnets on a stator structure generate the six magnetic fields that cross the coils. The wide magnetic gaps of the Lorentz actuators allow six-degree-of-freedom (6-DOF) motion of the flotor, with a motion range of ± 3 mm and $\pm 5^\circ$ from a nominal

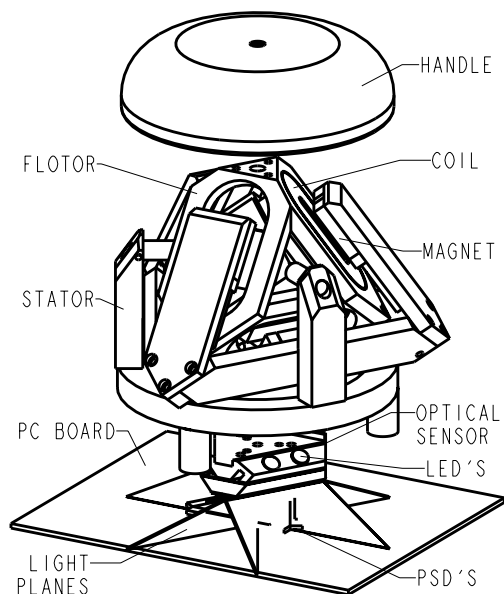


Figure 2: Schematic of the PowerMouse mechanical design.

center.

An optical 6-DOF sensor detects the flotor motion with a resolution of approximately 10 microns and 0.05 degrees. The sensor uses three LED-generated infrared light planes projected in sequence on three linear position sensing diodes (PSDs), mounted as an equilateral triangle on the PowerMouse printed circuit (PC) board. Each light plane crosses two PSDs. Thus six light-plane intersections with PSDs are obtained, allowing for the solution of the handle location using a direct kinematics computation.

The peak force of the device is 34 N, and the maximum continuous force is of the order of 16 N. The actuators have been optimized to maximize the force to power consumption ratio. It has been experimentally verified that, a result of the optimized actuators, the device operates far below its power capability suggesting that a larger workspace could be obtained by increasing the magnetic gaps. Should a large-motion range device be found necessary as a result of ergonomic studies, a haptic “pen” as described in [12] could be used.

2.4 Damping and dynamic performance

The dynamic performance of the robot and haptic interface is highly dependent on the damping coefficient of the controller. For all digitally controlled robots, the damping coefficient has an upper bound imposed

by discretization [2, 8]. When the control sampling frequency is fixed, the upper bound of the damping coefficient b_a at the actuator side is proportionally determined by the equivalent mass of the actuator and its inertial load $m_a + m_l$, $b_a = \alpha(m_a + m_l)$. The damping imparted to the load is $b = n_t^2 b_a = n_t^2 \alpha(m_a + m_l)$, where n_t is the transmission ratio. For direct drive robots in which the motor shaft is rigidly fixed to the joints, $n_t = 1$ but the inertial load seen by the actuator is $m_a + m_r$, where m_r is the equivalent robot mass at the joint of the actuator. Since m_r is large, it is easy to provide sufficient damping for good dynamic performance. When transmissions are used between the robot joints and the actuator shafts, any backlash will virtually disconnect the actuators from their inertial load. The equivalent mass seen by the actuator is just m_a , and the damping provided to the joint is $b = n_t^2 \alpha m_a$, which is usually small for n_t small. Thus, there is an inherent design tradeoff between achieving limited static forces for intrinsically safe operation, and good dynamic performance. The only way to avoid this trade-off is to use an additional means to provide damping, either by physical dampers or analog electronic dampers. This is consistent with the recommendation in [2] to achieve stiff virtual walls in haptic interfaces. Transmission elasticity, as found in cable transmissions, has a similar detrimental effect on achievable damping.

3 Control

A signal flow diagram and the present hardware implementation for the teleoperation system are illustrated in Fig. 3. During the ultrasound examination, the operator controls the ultrasound machine as usual, but moves a hand-controller or joystick instead of the ultrasound probe. Some of the control modes that have been tested or are envisaged are: **Master-slave mode without force feedback**, with the ultrasound transducer velocity and force tracking a joystick displacement as described in the next subsection. A SpaceMouse/Logitech Magellan [5] was used as a joystick. Experimental results are described below

Master-slave mode with force feedback, as described in [18], using the hand-controller described in [9]. Feasibility experiments using the control approach described below have been carried out [18]. **Shared operator/robot controller mode**, in which the two modes specified above might be used along some of the degrees of freedom, but not others.

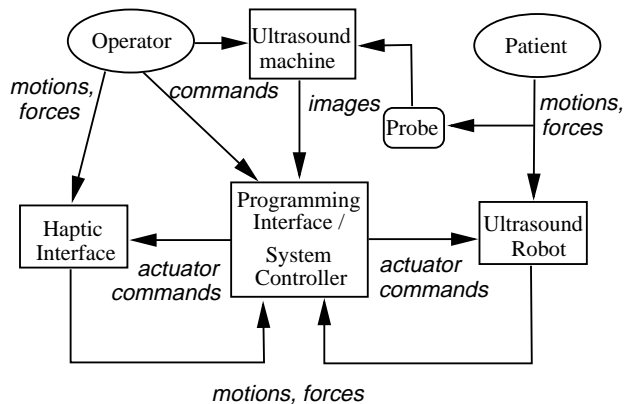


Figure 3: Signal flow for the teleoperation system

For example, the probe force along its beam center axis z_f could be controlled or kept within safe pre-specified values by the robot controller.

Shared operator/robot controller/image processor control, in which visual servoing can be used to control up to three degrees of freedom - the translation and rotation of the ultrasound transducer in the plane of the ultrasound beam, while the operator and robot controller control the other degrees of freedom. The image Jacobian obtained below demonstrates that indeed the three degrees of freedom in the ultrasound image plane are controllable.

3.1 Unilateral force/velocity control

The control approach is illustrated in Fig. 4. Its objective is to let a linear combination of the ultrasound probe velocity and scaled force track the joystick command (displacement), i.e.

$$\dot{X} + K_f F = \text{Command}, \quad (1)$$

where $\dot{X} \in R^6$ denotes the linear/angular velocity of the end-effector and K_f is a force scaling matrix. When in free motion where F is small the robot velocity tracks the command. In contact motion where \dot{X} is small, the contact force follows the joystick command divided by K_f . There is no explicit switching between the contact and free motion states. Experimental results for motion in the vertical direction are shown in Figure 5. A joint-space PID controller with saturated integral terms and mass and acceleration feedforward was used. An added layer of safety is insured by including in the control a “command reset” or “disturbance accommodation” function that never allows position errors to be large. Under normal operation,

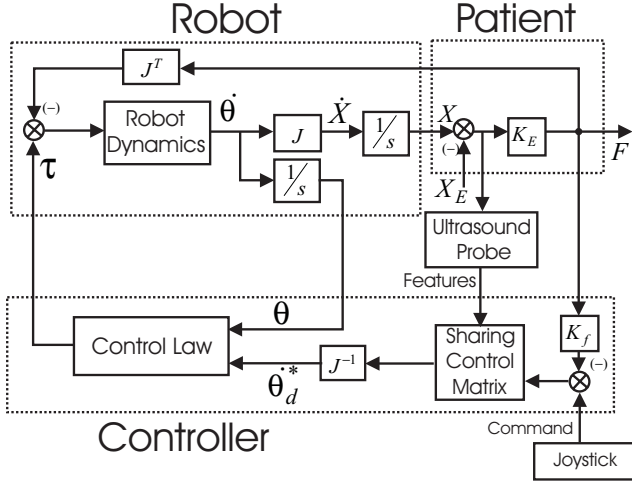


Figure 4: Velocity/force control

joint position errors are encompassed by a tolerance sphere of known radius. When this tolerance radius is exceeded, the command value is projected back into the tolerance sphere. Should the patient or the ultrasound technician attempt to push the robot out of the way, the robot will follow with little resistance due to its natural low impedance. Should the robot return to normal operation, it will stay close to where it was released. Note that the reset function does not require force sensor input and does not interfere with the ability of the robot to place the ultrasound probe accurately. Since the proportional and integral control terms are not allowed to increase, wind-up effects, such as the robot swinging when the patient's push subsides, do not exist.

Adaptive versions of the above control scheme can be developed by employing the virtual decomposition approach presented in [17]. The approach in [17] employs a sliding surface specified as a control target and model-based feedforward in which parameter estimates are used only plays a subsidiary role. Therefore, the system performance is not susceptible to large transient swings.

3.2 Adaptive bilateral motion/force control

A new teleoperation controller has been developed to deal with unknown operator hand and patient environments. As illustrated in Figure 6, in this approach, the master and slave robots are controlled independently by the adaptive motion/force controller reported in [17], and are L_2 and L_∞ stable:

$$(V_{\gamma d} - \dot{X}_\gamma - A\tilde{F}_\gamma) \in L_2 \cap L_\infty \quad (2)$$

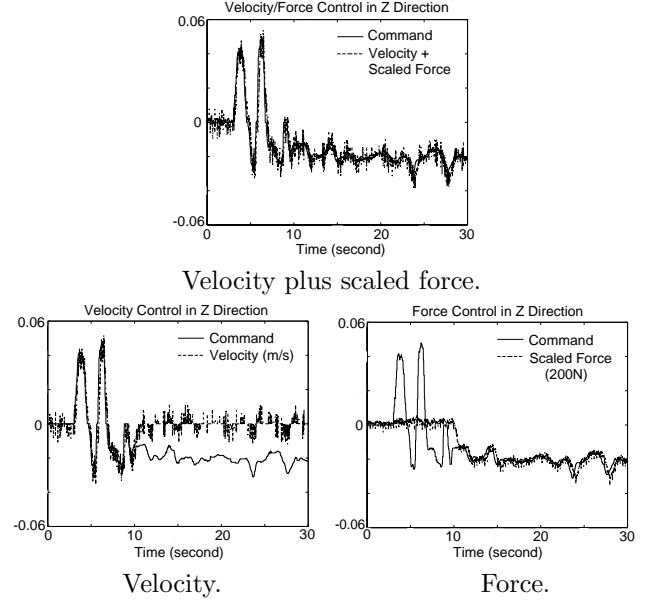


Figure 5: Tracking under motion/force control.

where the index γ is h for the master and e for the slave, and $V_{\gamma d}$, \tilde{X}_γ are desired and actual velocities, A is a constant gain determining the relative scaling between force and velocity tracking, and \tilde{F}_γ are filtered forces applied by the operator/environment on the master and slave robot. The usual linear-in-parameters models are assumed for the two robots [17], and the operator and environment are assumed to be linear time-invariant second-order systems. None of the model parameters have to be known. The parameters do not converge in general, but are bounded. To achieve bilateral teleoperation with L_2 and L_∞ stability, the master and slave command signals are designed as follows [18]:

$$\begin{aligned} \dot{X}_{ed} &= K_p \tilde{X}_h + \lambda(K_p \tilde{X}_h - X_e) - A K_f \tilde{F}_h \\ \dot{X}_{hd} &= \frac{1}{K_p} \left\{ \tilde{X}_e + \lambda(\tilde{X}_e - K_p X_h) \right. \\ &\quad \left. - A[\tilde{F}_e + (K_f - K_p)\tilde{F}_h] \right\} \end{aligned}$$

where K_p and K_f are motion and force scaling parameters, and (\tilde{s}) denotes a first-order filtered version of s . This controller has a fixed four-channel architecture, with the parameter adaptation performed by the internal controllers of the master and the slave. It has been shown in [18], that

$$\begin{aligned} \rho_p \triangleq K_p \dot{X}_h - \dot{X}_e &\in L_2 \cap L_\infty \\ K_p X_h - X_e &\in L_2 \cap L_\infty . \end{aligned}$$

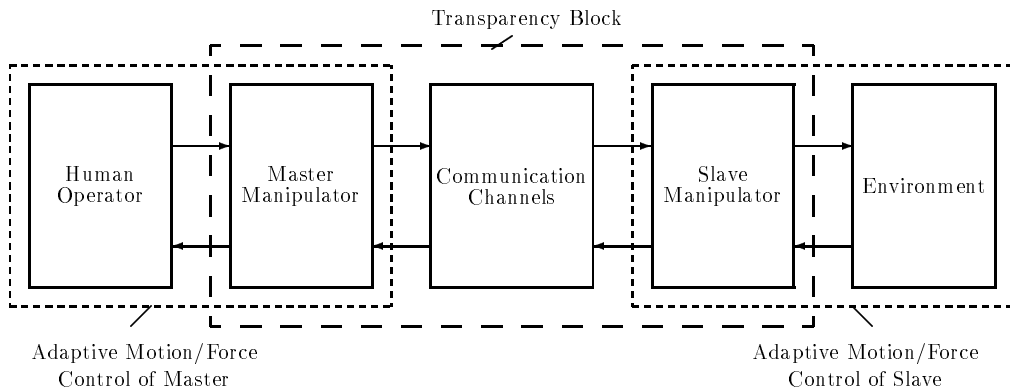


Figure 6: Teleoperation with adaptive motion/force control.

Furthermore, the teleoperation system transmits to the operator the environment impedance appropriately scaled by the position and force gains, and an additional mass-damper impedance that depends on the controller parameters. In the scalar case, the impedance transmitted to the hand is:

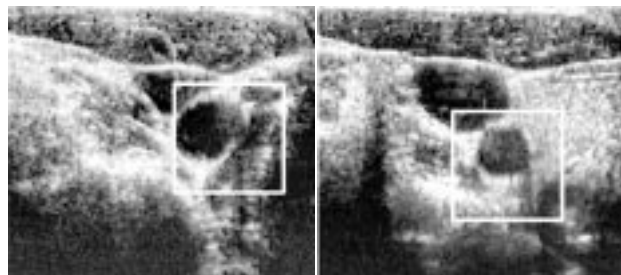
$$-Z_h = \frac{K_p}{K_f} Z_e + \frac{K_p}{K_f} \frac{s + \lambda}{AC}. \quad (3)$$

Experimental results have shown excellent position and force tracking and robustness to delays of up to 1-2 seconds.

3.3 Visual Servoing and Feature Tracking

Visual servo-control [3] could be used to control motion in the plane of the ultrasound beam. Its feasibility is determined by the ultrasound image Jacobian J_v , which relates differential changes in image features to differential changes in the end effector location [3]. The rank of the J_v is at most three, and will be equal to three for two or more feature points non-collinear with the origin [11]. Thus, as expected, with non-trivial ultrasound images, it is possible to control the motion of the ultrasound transducer in its image plane.

A number of motion tracking algorithms have been implemented to evaluate the feasibility of ultrasound image servoing. In a modified cross-correlation technique, the best correlation was sought between the current frame and frames at times $t_k, t_{k-2}, t_{k-4}, \dots, t_{k-2n}$, where n is fixed. This method leads to little drift, since the reference frame is not fixed, and shows some robustness to changes in the image. Two feature-based methods were also implemented - the star algorithm and discrete snakes, in which the carotid artery

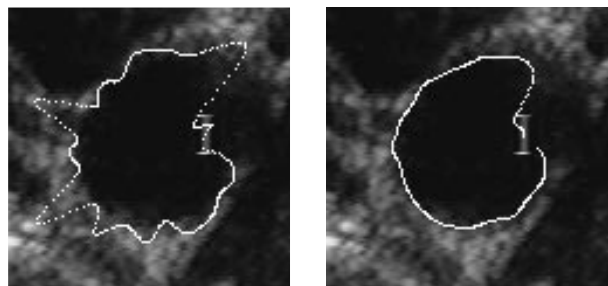


Initial image.

Image after 10 seconds.

Figure 7: Tracked carotid artery image using a modified correlation algorithm.

boundary is sought. The star algorithm uses an edge-detection filter to detect the carotid artery boundary along rays emanating from a point interior to the carotid artery, while the discrete snake method minimizes an energy function between a closed curve and points detected via the star algorithm. The results are summarized in Table 2, and the carotid artery as recognized by the star and snake algorithms are shown in Figure 8.



Star algorithm.

Discrete snake algorithm.

Figure 8: Carotid artery boundary determination.

Method	Correlation	Star	Snake
Average tracking time (sec.)	5-10	10-20	10-15
Max. tracking time(sec.)	30	50	40
Computational Cost (kflops)	100	30-150	50-300
Stability	Medium	Low	High
Border accuracy	N/A	Medium	High

Table 2: Performance comparison of different motion tracking algorithms. Image sub-blocks of 128 x 128 pixels have been used.

4 Discussion and challenges

Regardless of whether the robot-assisted ultrasound system described in this paper becomes a useful clinical tool, its development points to a number of research challenges in the area of assistive and human augmentation devices. These require contributions from several disciplines:

Human-dependent specifications. The first challenge encountered is the dependency of specifications on people. Although the tolerances on specifications can be looser than encountered in manufacturing problems, studies of human capabilities and actions require appropriate instrumentation [10] and studies with several to many subjects. In addition, there are instances in which the design of robots or teleoperation systems may be affected by human factors studies. For example, [6] evaluates the effect of motion constraints on the performance of tasks typical of laparoscopy. The results allow a designer to select the number of degrees of freedom that are used in an endoscopic teleoperator as a function of task completion times.

Radical design ideas may also be proven or disproven by human factors studies. For example, [15] evaluates the feasibility of using a moving hand support, essentially a movable bracing platform, to enable a surgeon to perform coronary bypass on the beating heart. Surprisingly, the study [15] shows that if a system could be developed that tracks a moving task site perfectly, subjects could perform delicate tasks *with their hands in motion* with only a 10% loss in accuracy and 40% loss in completion time relative to the case where the task and hands are still.

Design for safety. The ultrasound robot design illustrates the difficulty of designing mechanisms that can be safely manipulated by people at reasonable speeds and accelerations. In particular, note the difficulty of achieving effective damping at low transmission ratios.

Controller design and tuning. Most control schemes require significant tuning to work reliably. Reliable parameter adaptation/learning schemes are necessary to allow multiple users without designer intervention.

Ergonomic interfaces. Multiple control modes as encountered in this system for ultrasound will be more and more common. They require the fusion of multiple channels of sensory data to present to the operator, and the interpretation of possible conflicting commands from the operator in order to produce a desirable outcome.

Effectiveness. The convincing demonstration of the benefits of a system require again human factors studies, and these have to be fairly extensive in the area of medical devices. The effort required for the simplest of tasks is substantial [10].

5 Conclusion

We have presented a robot system for medical ultrasound. A safe, light, counterbalanced robot was designed to perform ultrasound examinations of the carotid artery. The robot was controlled in a motion/force mode that allows a seamless switch between rate and mode control. A suitable teleoperation controller that is stable, transparent and can adapt to multiple operators and environments has been presented. The feasibility of ultrasound image servoing has been demonstrated with a number of image processing algorithms. Shared control methods between motion/force/visual control have been presented. The system requirements are representative of the range of problems that need to be solved for effective collaboration between humans and machines, and can serve as a test-bed for control and interface research work.

6 Acknowledgments

Discussions with Prof. David Lowe and Dr. Paul Trepanier, help with imaging from Henry Wong, machining and robot construction by David Fletcher and

Peter Vautour are gratefully acknowledged. This work is supported by the Canadian IRIS Network of Centres of Excellence project SAL.

References

- [1] J. F. Brinkley, W. E. Moritz, and D. W. Baker. Ultrasonic three-dimensional imaging and volume from a series of arbitrary sector scans. *Ultrasound in Medicine and Biology*, 4:317-327, 1978.
- [2] Colgate, J.E., Grafing, P.E., Stanley, M.C., and Schenkel, G., 1993. Implementation of stiff virtual walls in force-reflecting interfaces. In *IEEE Virtual Reality annual international Symposium*, pages 202–208.
- [3] P. I. Corke, *Visual Control of Robots: High Performance Visual Servoing*, John Wiley & Sons Inc., 1996.
- [4] M. Craig, "Sonography: An occupational health hazard?," *Journal of Diagnostic Medical Sonography*, vol. 1, pp. 121–124, May/June 1985.
- [5] Hirzinger, G., Dietrich, J., Gombert, B., Heindl, J., Landzettel, K., Schott, J., "The sensory and telerobotic aspects of the space robot experiment ROTEX," in *Int. Symp. on Artificial Intel., Rob. and Aut. in Space*, (Toulouse, France), Sept. 30- Oct. 2, 1992.
- [6] A.J. Hodgson, J.G. Person, S.E. Salcudean and A.G. Nagy, "The Effects of Physical Constraints in Laparoscopic Surgery", *Medical Image Analysis*, pp. 275-283, 3(3), 1999.
- [7] F Pierrot, E Dombre, E Dgoulange, L Urbain, P Caron, S Boudet, J Garipy and JL Mgnien "Hippocrate: a safe robot arm for medical applications with force feedback", *Medical Image Analysis*, pp. 285-300, 3(3), 1999.
- [8] S.E. Salcudean and T. Vlaar, "On the Emulation of Stiff Walls and Static Friction with a Magnetically Levitated Input-Output Device", *ASME Journal of Dynamic Systems, Measurement and Control*, 119:127-132, March 1997.
- [9] S.E. Salcudean and N.R. Parker, "6-DOF Desk-Top Voice-Coil Joystick", *6th Annual Symposium on Haptic Interfaces for Virtual Environments and Teleoperation Systems, Intl. Mech. Eng. Congr. Exp., (ASME Winter Annual Meeting)*, DSC-Vol. 61, pp. 131–138, Dallas, Texas, November 16-21, 1997.
- [10] S.E. Salcudean, S. Ku and G. Bell, "Performance Measurement in Scaled Teleoperation for Microsurgery", *Proceedings of the joint CVRMed and MR-CAS Conference*, La Tronche, France, March 20-22, 1997. (Note duplicate entry - this appears as a book chapter below, but it was refereed.)
- [11] S.E.Salcudean, G.Bell, S. Bachmann, W.H. Zhu, P. Abolmaesumi and P.D. Lawrence, "Robot-Assisted Diagnostic Ultrasound - Design and Feasibility Experiments", *MICCAI'99, Second Intl. Conf.*, pp. 1063-1071, Cambridge, U.K., Sept. 1999.
- [12] L. Stocco, S.E. Salcudean and F. Sassani, "Mechanism Design for Global Isotropy with Applications to Haptic Interfaces", *6th Annual Symposium on Haptic Interfaces for Virtual Environments and Teleoperation Systems, Intl. Mech. Eng. Congr. Exp., (ASME Winter Annual Meeting)*, pp. 115–122, Dallas, Texas, November 16-21, 1997.
- [13] J. W. Sublett, B. J. Dempsey, and A. C. Weaver. Design and implementation of a digital teleultrasound system for real-time remote diagnosis. In *Proceedings of the 1995 Symposium on Computer-Based Medical Systems*, pages 292-298, 1995.
- [14] R. H. Taylor, J. Funda, B. Eldridge, S. Gomory, K. Gruben, D. LaRose, M. Talamini, L. Kavoussi, and J. Anderson. A telerobotic assistant for laparoscopic surgery. *IEEE Engineering in Medicine and Biology Magazine*, 14(3):279-288, May/June 1995.
- [15] A.L. Trejos, S.E. Salcudean, F. Sassani, and S. Lichtenstein. "On the feasibility of a moving support for surgery on the beating heart." *MICCAI'99, Second Intl. Conf.*, pp. 1088-1097, Cambridge, U.K., Sept. 1999.
- [16] H. E. Vanderpool, E. A. Friis, B. S. Smith, and K. L. Harms, "Prevalence of carpal tunnel syndrome and other work-related musculoskeletal problems in cardiac sonographers," *Journal of Occupational Medicine*, vol. 35, pp. 604–610, June 1993.
- [17] W. H. Zhu, Y. G. Xi, Z. J. Zhang, Z. Bien, and J. De Schutter, "Virtual decomposition based control for generalized high dimensional robotic systems with complicated structure," *IEEE Trans. Robotics and Automation*, vol.13, no.3, pp.411-436, 1997.
- [18] W.H. Zhu and S.E. Salcudean, "Teleoperation with Adaptive Motion/Force Control", *1999 IEEE Intl. Conf. Rob. Aut.*, pp. 231–237, Detroit, USA, May 1999.
- [19] E.J. Chen, I.A. Hein, J.B. Fowles, R.S. Adler, P.L. Carson, and W.D. O'Brien Jr., "A Comparison of the Motion Tracking of 2-D Ultrasonic B-Mode Tissue Images with a Calibrated Phantom", *1991 IEEE Ultrasonic Symposium*, pp. 1211-1213.